Final Report on the Airborne Lidar component of the CIFAR project, "Investigation of the foraging behavior of Steller sea lions in the vicinity of Kodiak Island, Alaska"

James H. Churnside
NOAA Environmental Technology Laboratory
325 Broadway
Boulder, CO 80305

Tim Veenstra
Airborne Technologies
P.O. Box 879050
Wasilla, AK 99687

Abstract

The NOAA Fish Lidar was used to survey winter aggregations of herring in several areas of Kodiak Island in March, 2002. Herring were observed in Uganik Bay and Ugak Bay, in areas where Steller sea lions were observed visually. Sea lions, as well as sea birds, were also observed with visible and infrared imagers. However, the largest concentration of herring seen by the ship surveys was in the South Arm of Uganik Bay, and this concentration was not detected by the lidar. This result was completely unexpected. A similar concentration of herring in a similar bay in Prince William Sound was detectable by the lidar. During the summer prior to this study, the lidar was used to map fish distributions in a variety of locations around Kodiak Island, including inside several bays. The South Arm of Uganik Bay was found to have a very high level of dissolved organic material, even when compared with the rest of Uganik Bay. This produced absorption of the laser beam that was greater than we have seen in any other area.

Introduction

The overall objective of this program was to investigate the foraging behavior of Steller sea lions in the vicinity of Kodiak Island. The specific hypothesis was that these animals selectively feed on herring during the winter. This hypothesis was based, in part, on evidence that sea lions require fat-rich prey, such as herring or capelin, in their diet in order to thrive (Rosen and Trites, 2000). It was also based, in part, on observations of sea lions foraging on herring at night during the winter in Prince William Sound (Thomas and Thorne, 2001).

The survey techniques were designed after those that had been used in Prince William Sound. These include echosounders at 38kHz and 120 kHz, direct sampling of prey by purse seine and midwater trawls, visual and infrared predator surveys from surface vessel, airborne visual surveys, and airborne lidar surveys. Most of these techniques have a long history, and their strengths and weaknesses are well known. Airborne lidar is the exception. Most of these techniques were implemented by Richard Thorne and Gary Thomas of the Prince William Sound Science Center, and the results are presented in a separate report. Again, airborne lidar is the exception, and this report is a description of those results.

While several airborne visual surveys and several ship surveys were done throughout the winter, available resources allowed only one period for airborne lidar surveys in the winter. We decided to perform these surveys in March, 2001. This is late enough in the winter that the general regions of winter aggregation of herring would be known from ship and visual surveys, but early enough that the herring would still be in their winter habitat. From these earlier surveys, we knew that the majority of the herring around Kodiak Island were in the South Arm of Uganik Bay, with a smaller concentration in Ugak Bay. Our surveys concentrated in these areas. For comparison, some results of our March surveys in Prince William Sound will also be presented.

We were successful in mapping the distribution of herring in most of Uganik Bay and in Ugak Bay. However, we were not successful in detecting the largest group of herring in the South Arm of Uganik Bay. The reason is that the lidar only penetrated down to 8 – 9 m in this area, the least penetration we have observed in any location to date. A comparison of the lidar characteristics just outside of the South Arm with those inside of the Arm leads us to the conclusion that the waters there contain very high levels of dissolved humic acids. This is the first report of measurement of dissolved organic material using a single-frequency lidar.

It is not clear whether or not the lidar would have worked in this area earlier in the winter. The fact that spotter pilot reports were used to help determine that this was, in fact, an area where they were suggests that it might have. Any fish that can be seen by the pilots present a very strong return of the lidar. It is also not clear whether this level of dissolved organics is present in this area every year, or if this year was an exception.

The lidar worked well in detecting winter aggregations of herring in a similar bay in Prince William Sound, where the penetration depth was much greater. It also worked well in other studies around Kodiak Island done between May and September. Some of these studies were close to shore, although we never did revisit the South Arm of Uganik Bay during this work.

Instrumentation

The original plan for 2002 was to mount the lidar and imager on a US Coast Guard helicopter, which they had offered to provide. In the wake of the events of September 11, this was no longer possible, and another suitable helicopter could not be found within the constraints of schedule and budget. Instead the lidar was modified to operate over a broader range of flight altitudes with minimal loss of performance. It and the imager were then installed on a King Air 90 twin turbo-prop airplane. A photograph of the airplane is presented in **Figure 1**.

Figure 1. 2002 survey aircraft

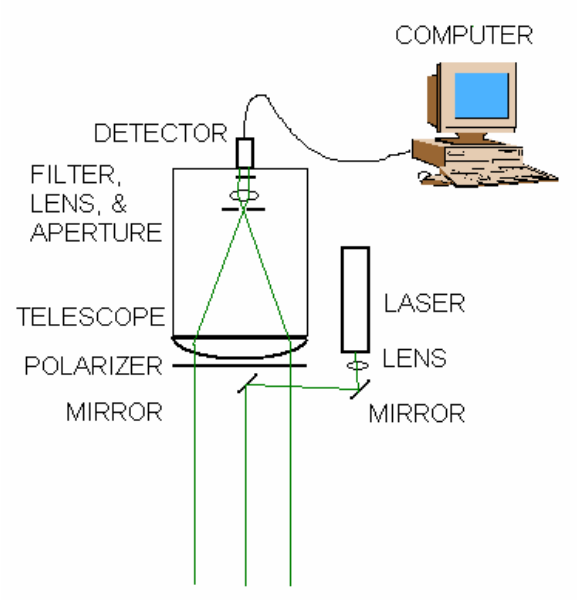

Figure 2 Schematic diagram of lidar

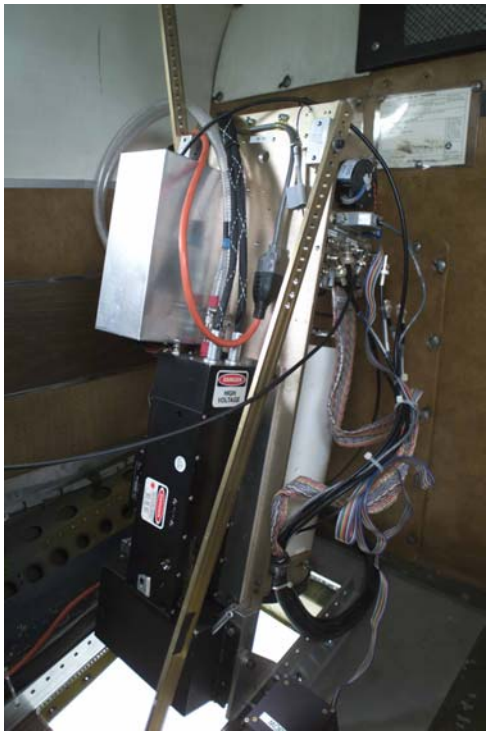

Figure 3 Lidar in aircraft

The lidar system is a non-scanning, radiometric lidar. A block diagram is presented in **Figure 2**. The major components are 1) the laser and beam-control optics, 2) the receiver optics and detector, and 3) the data collection and display computer. **Figure 3** is a photograph of the optics package installed in the airplane. The black box on the left near the bottom is the laser and a cover for the steering mirrors and diverging lens. The silver box near the top of the optics package is the power supply for the various components. The telescope is on the other side of the gold-colored plate. Both the telescope and the laser are directed downward through a hole in the bottom of the aircraft. Churnside, et al., (2001) present more details about the lidar.

The laser is a frequency-doubled, Q-switched Nd:YAG laser that produces about 100 mJ of green (532 nm) light in a 12-nsec pulse at a rate of 30 pulses per second. The laser is linearly polarized and the beam is diverged, using a lens in front of the laser, so that it is safe at the surface (ANSI, 1993). This irradiance level is also safe for marine mammals (Zorn, et al., 2000).

The diverged beam is directed by a pair of mirrors to be parallel to the axis of the telescope. The figure shows a coaxial configuration of the transmitter and receiver. For these flights, a side-by-side configuration was used instead. While the coaxial configuration makes alignment easier at the short ranges available inside an aircraft hanger, there is no difference in the performance of the two configurations in flight.

The receiver optics use a 17-cm-diameter refracting telescope. A polarizer is placed on the front of the telescope to select either the component of the return that is co-polarized with the laser or the cross-polarized component. We used the cross-polarized component, because our experience suggests that this component produces the best contrast between fish and the scattering from small particles in the water. The telescope collects the light onto an interference filter to reject background light. An aperture at the focus of the primary lens also limits background light by limiting the field of view of the telescope to match the divergence of the transmitted laser beam. The resulting light is incident on a photomultiplier tube (pmt), which converts the light into an electrical current. A 50-Ω load resistor converts the current in a voltage, which can be digitized in the computer.

High-speed digitizers exist that plug directly into the bus of personal computers, but these are limited to 8 bits of resolution. This produces 255 possible levels, which is not as much dynamic range as we would like for fish lidar applications. Therefore, we fed the detector output into a logarithmic amplifier. The output of the logarithmic amplifier is fed into the digitizer. The particular amplifier we used has a response of

$$V_{\log} = -0.125 \log_{10}(-V_{linear}) - 0.486. \quad (1)$$

It has an input voltage range of -0.2 mV to -2 V, which corresponds to an output voltage range of about -0.024 V to -0.524 V. Since the output voltage range is well within the

range of an 8-bit digitizer, the logarithmic amplifier increases the maximum possible dynamic range from 255 to about 10^4.

The computer records the raw lidar data. It also records aircraft position from the aircraft Global Positioning System (GPS), GPS time, the voltage applied to the photomultiplier tube, and the attitude of the aircraft as measured by tilt meters and laser gyroscopes on the optical package. The applied voltage on the photomultiplier tube is used to find the gain of the tube, which is necessary for calibration. The computer is also used to display the data during the flight.

The thermal imager is a Raytheon IR2000B, which has an un-cooled ferroelectric detector (320x240) sensitive from 7 to 14 microns. A thermoelectric cooler provides thermal stabilization. The imager outputs an SMPTE-170M video signal that is recorded onto digital video tape. The video is updated at a 30 Hz rate. A computer controls the imager via an RS-232 serial communication port. A 50-mm lens on the imager provides a 18x13.5 degree field of view. The imager is mounted on a gyroscopically stabilized mount that is affixed to the floor of the aircraft over a camera port that looks straight down with a nadir point of view. **Figure 4** is a photograph of the thermal imager and a color video camera taken from below the aircraft. The thermal imager is the one with the shiny lens.

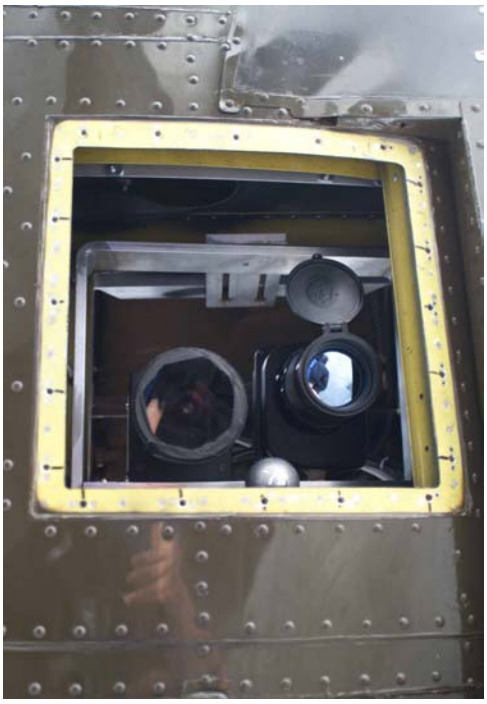

Figure 4. Thermal camera from below

At the same time the video signal is recorded onto digital video tape, GPS information of the flight track is being recorded onto one of the two available sound tracks. A 9-inch black and white monitor enables the operator to view the thermal imager signal in real time. Any item of interest can be "marked" on the GPS track by an external trigger connected to the computer. This enables fast post-process review of suspected targets. The second sound track of the DV recorder is used to record all aircraft intercom and radio communications. This communications recording aids in post process correlation between the lidar and imaging data with what the aircraft and vessel personal are viewing.

A 3-chip digital video camera was mounted in the aircraft to aid in target identification during day flights. The signal was displayed in real time on a 9-inch color monitor and was also recorded on digital video tape in the same way as the thermal video. The 3-chip color video camera is also shown in **Figure 4**.

Flight Summary

The weather in South-Central Alaska can be somewhat unsettled in March. Low flight altitudes increase the chances of doing a survey below the clouds, but it is not safe to fly a fixed wing aircraft under the clouds into a narrow bay like Uganik when the mountains are in the could all around and there is not room to turn around. This made it difficult to get into Uganik Bay while the ship survey was in progress, but we were able to make a good day and night survey shortly after the ship survey. The areas of interest in Prince William Sound are more open, and we made 2 day and night surveys separated by about a week. All flights are summarized in Table 1.

Table 1. Summary of flights in March, 2001.

Date	Location	Day or Night	Altitude (feet)
3/14	Ugak Bay	Day	1000
3/18	Uganik Bay	Day	5000
3/21	Prince William Sound	Day	3500
3/21	Prince William Sound	Night	3500
3/22	Prince William Sound	Day	1000
3/28	Prince William Sound	Day	1000
3/28	Uganik Bay	Day	1000
3/28	Uganik Bay	Night	5000
3/28	Ugak Bay	Night	5000
3/29	Prince William Sound	Night	2000

The first flight was made over Ugak Bay under the clouds. We saw returns from a couple of small schools, kelp, and at least one large animal. No significant concentrations of herring were seen, however, and the results of this flight will not be described in detail. The next flight, over Uganik Bay, was interrupted by clouds. The interesting part of the bay could not be covered, and these results will not be presented in detail either.

Lidar Results

Uganik Bay, Kodiak

The greatest concentration of herring around Kodiak Island was expected to be in the South Arm of Uganik Bay. No fish were detected by the lidar in this region either during the day flight or the night flight. The probable reason is that the depth penetration was only 7 – 8 m, day or night. This is a very unusual condition, and is discussed further below.

Distinct schools of fish were seen near East Point, and birds and sea lions were observed visually in this same area. Distinct schools were also seen in shallow water. **Figure 5** is a map of the distribution of scattering for the day flight in Uganik Bay. The

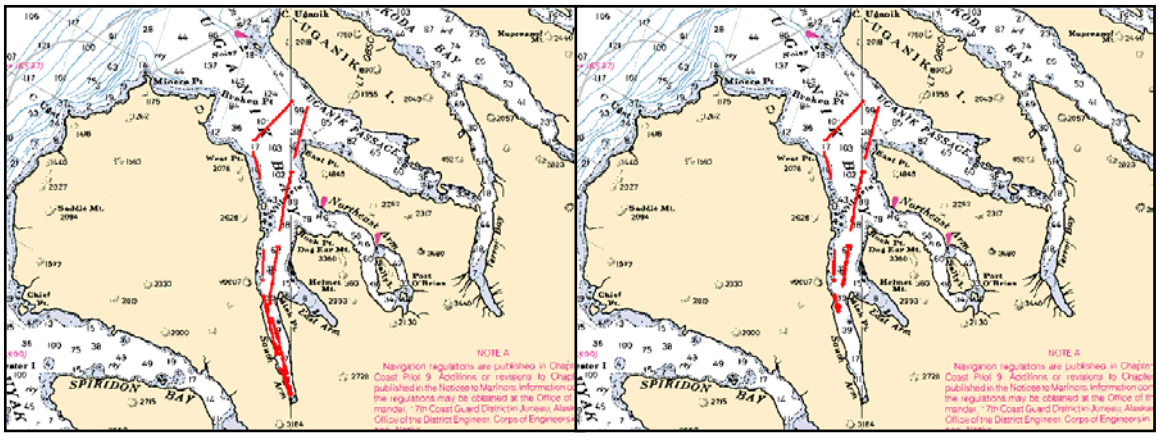

a. 0 – 5 m b. 5 – 10 m

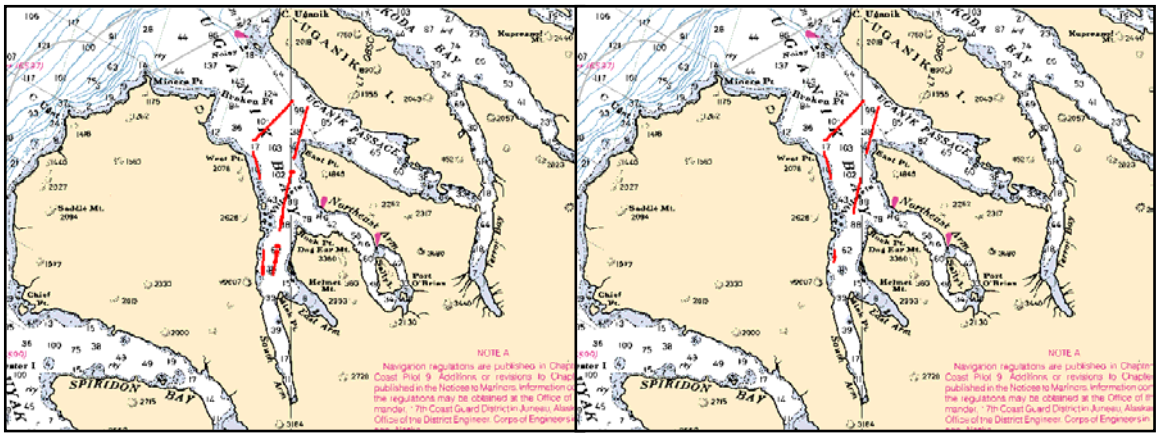

c. 10 – 15 m d. 15 – 20 m

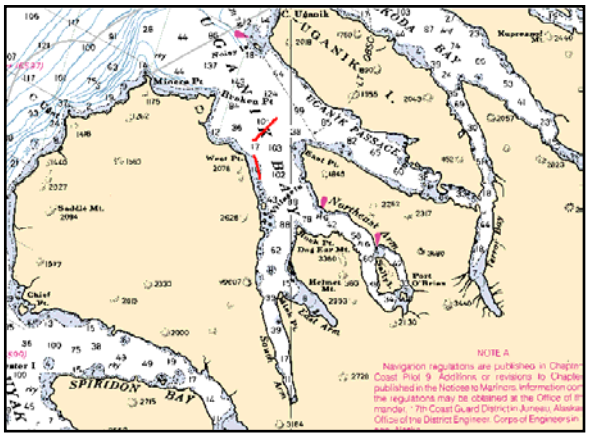

e. 20 – 25 m

Figure 5. Distribution of lidar energy by depth in and around the Uganik Bay for the day of March 28.

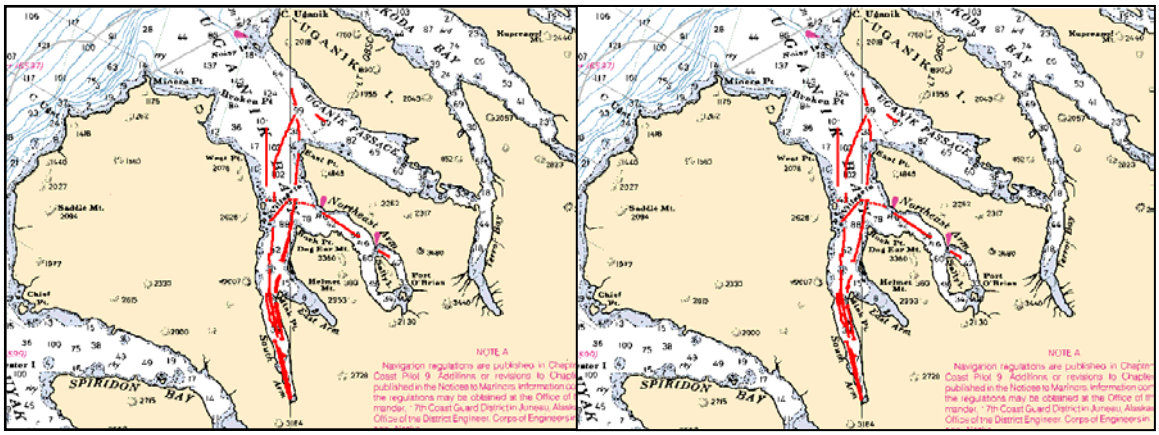

a. 0 – 5 m b. 5 – 10 m

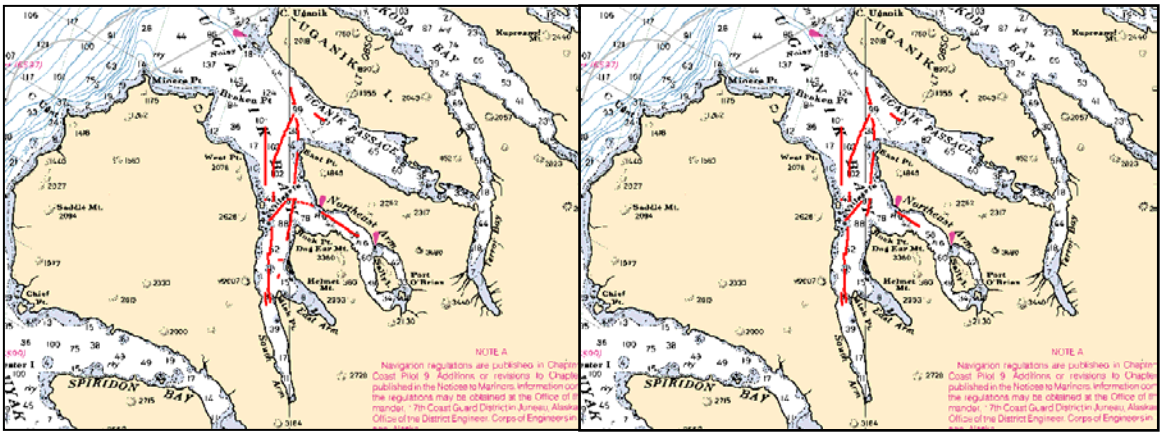

c. 10 – 15 m d. 15 – 20 m

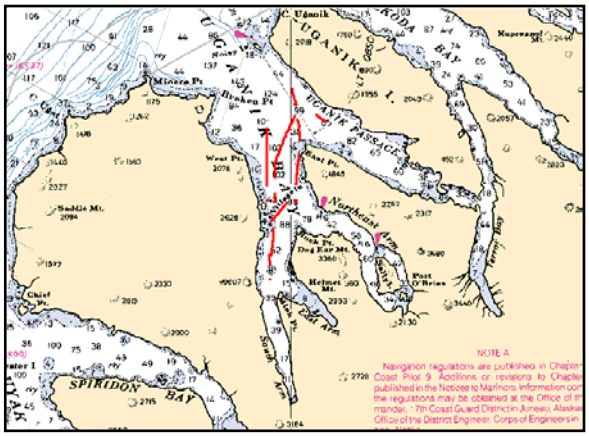

e. 20 – 25 m

Figure 6. Distribution of lidar energy by depth in and around the Uganik Bay for the night of March 28.

main features are a surface scattering layer in South Arm and several small areas with fish schools between 5 and 15 m outside of South Arm. **Figure 7** is an echogram of one of these school groups near East Point. Sea birds and several sea lions were observed visually in this same area.

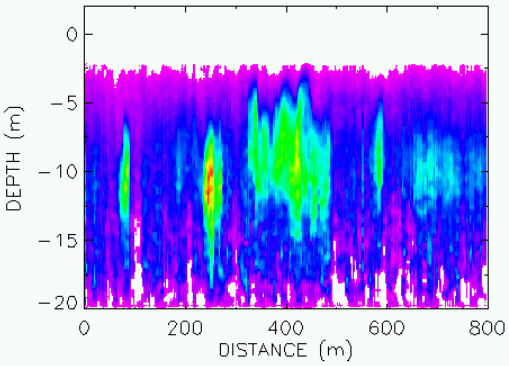

Figure 7. Daytime echogram of school group near East Point in Uganik Bay.

Figure 6 is a map of the distribution of scattering for the flight that same night. No concentrated schools were observed. A diffuse scattering layer was observed in the area near East Point. An echogram of a section of this layer is presented in **Figure 8**. There is structure within the layer, but it is much larger and more diffuse than the school structure seen during the day. The infrared camera recorded birds in this same area. Based on the nighttime results of Thorne and Thomas in Prince William Sound, we expected that the infrared camera might also show congregations of sea lions during the night flight, but none were observed.

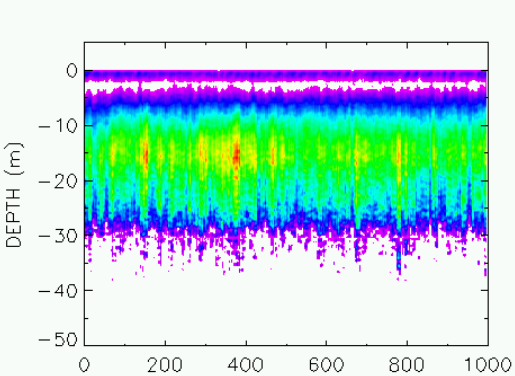

Figure 8. Nighttime echogram of layer near East Point in Uganik Bay.

There was a very distinctive change in the absorption of the laser beam at the mouth of the South Arm, probably caused by a high level of dissolved organic material (DOM). **Figure 9** is a plot of average lidar

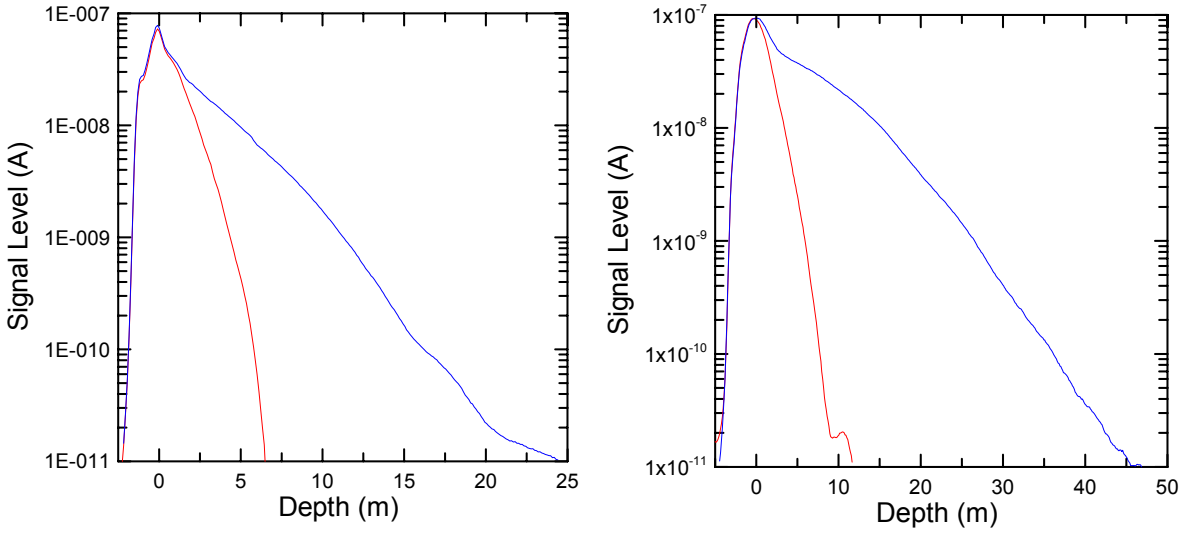

Figure 9. Average lidar return profiles inside (red) and outside of (blue) South Arm during the day (left) and at night (right).

return over about 1000 m in the center of South Arm and another average outside the arm, near East Point. We see that the surface signal is nearly identical in both areas. This suggests that the concentration of scatterers in the water is nearly equal, at least near the surface. However, the attenuation is very different. During the day, we are seeing down to about 20 m outside of South Arm, but only to about 7 m within the Arm. At night, the penetration increases to over 40 m in the outside area, but only to about 9 inside. We conclude that the high attenuation in South Arm must be due to a much greater absorption in that area. Higher absorption without a corresponding higher level of scattering suggests a high level of dissolved organic matter.

The edge of the absorbing water was a very sharp feature right at the mouth of South Arm. There was a distinct surface temperature difference at the same location, as measured by an infrared radiometer on the aircraft. The conclusion is that there is little mixing of the water within South Arm and that outside of it, at least at this time of year.

The most likely cause of the absorption is dissolved humic substances washed into the Arm from the surrounding land. We can estimate the concentration of this substance from the attenuation. Table 2 lists the attenuation averaged from 2 – 3 m using the data in **Figure 9**. We assume that the attenuation outside the Arm provides an estimate of the contributions from pure water (about 0.05 m^{-1}) and from particles, with a relatively small contribution from DOM. The difference between the inside and outside attenuation is taken to be an estimate of the attenuation by DOM within the Arm. From the measured attenuation at 532 nm, we estimate the attenuation at 450 nm using the relationship (Twardowski and Donaghay, 2002; Blough, et al., 1993; Bricaud, et al., 1981; Carder, et al., 1989):

$$\alpha(\lambda) \quad = \quad \alpha(\lambda_0)\exp\left[-0.014(\lambda - \lambda_0)\right],$$

where α is the attenuation coefficient, λ is the wavelength of interest (in nm), and λ_0 is the wavelength for which the attenuation is known.

Table 2. Attenuation coefficients and concentration of dissolved carbon within the South Arm.

	α(532) inside	α(532) outside	α(450) inside	α(450) outside	C (mg l^{-1})
Day	0.494	0.158	1.56	.50	1.63
Night	0.396	0.119	1.25	0.38	1.34

The DOM absorption is estimated to be about 0.3 at 532 nm from the data in Table 2. It is interesting to compare this value with measurements at other locations. Mobley (1994) presents a table of DOM absorption coefficients at 440 nm. For comparison, we can convert these to 532 nm using the equation above. The highest oceanic value is a value of 0.031 in the Gulf of Guinea, approximately an order of magnitude lower. The highest estuarine value is 0.18 in the Clyde River estuary in Australia, still about a factor of two lower.

The measured absorption value is used to estimate the amount of dissolved carbon in the DOM using a value of 0.65 m^{-1} (mg l^{-1})$^{-1}$ (Twardowski and Donaghay, 2002). The day and night values are presented in Table 2. The average value is about 1.5 mg l^{-1}. Blough, et al. (1993) measured values about twice this in the fresh water of the Orinoco River estuary. They estimate that this discharge accounts for about 1% of the total global transport of dissolved organic carbon into the ocean. From these comparisons, we conclude that the level of DOM in South Arm is significantly higher than one might reasonable expect.

Ugak Bay, Kodiak

During the two flights over Ugak Bay, fish were only detected along the north shore. The positions are presented in **Figure 10**. Most were in fairly shallow water. The day flight was about 2 weeks before the night flight, and the observed schools were farther up in the bay. The nighttime observations were closer to the mouth of the bay. They were also in larger layers with less internal structure. This latter feature can be seen in echograms of a daytime (**Figure 11**) and nighttime (**Figure 12**) school.

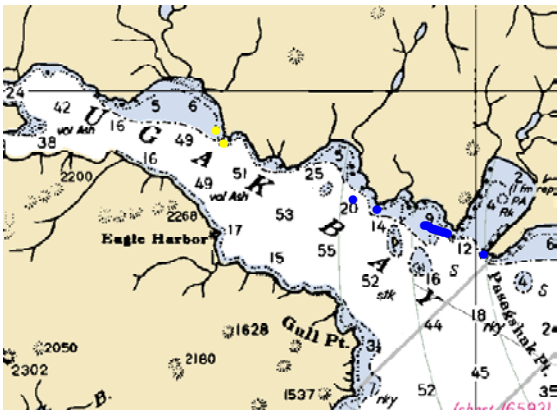

Figure 10. Locations of fish schools in Ugak Bay during the day of March 14 (blue) and the night of March 28 (yellow).

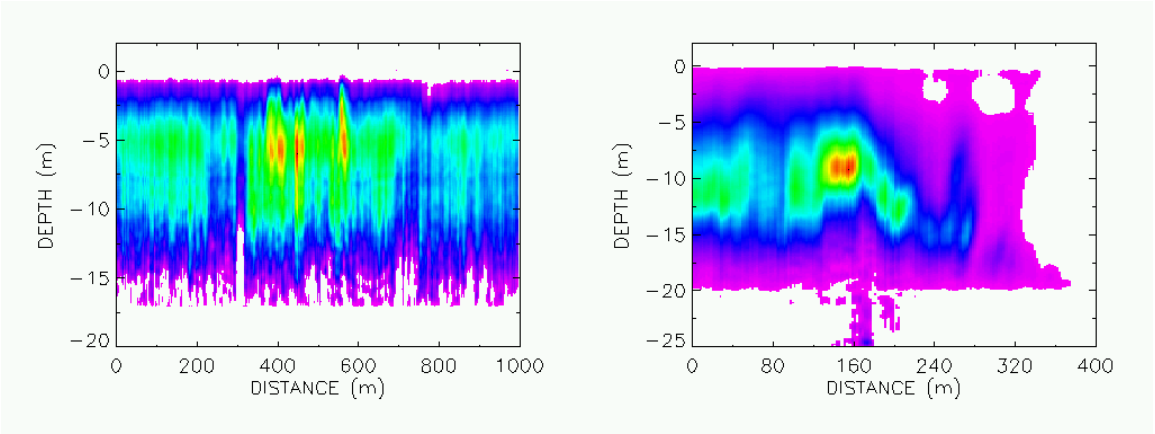

Figure 11. Echogram of daytime school group in Ugak Bay.

Figure 12. Echogram of nighttime school group in Ugak Bay.

Zaikov Bay, Prince William Sound

For comparison, we consider the lidar results from Zaikov Bay. Like the South Arm of Uganik Bay, this are was known to be a major wintering area for herring. **Figures 13 - 16** (starting on the next page) are maps of the distribution of scattering in and around Zaikov Bay. Four flights were made over the bay – a day and night flight on March 21 and 22 and another set about 1 week later. The four maps present the results from these four flights. In all cases, significant lidar backscatter was found from near the surface down to about 15 m in the head of the bay. The levels were higher on the first pair of flights than on the second. This is consistent with observations on the second flight of herring spawn in Port Gravina and of surface schools of herring outside of the Bay near Green Island. It suggests that the fish have started to move out of their winter areas.

Figure 17 is a typical echogram of the lidar backscatter from the head of the bay. On all four flights, the lidar return was a strong layer with a lot of structure within the layer. **Figures 18** and **19** show the typical structure of the layer within the bay compared with the profile of lidar backscatter outside of the bay. Each is the average of about 1000 m along the flight track. In both the day and night cases, the backscattering is stronger and more broadly distributed in depth in the earlier flights than in the latter. The depth of the layer does not seem to change much from day to night. The attenuation inside the Bay and outside is similar in all cases, suggesting that there is not a greatly increased concentration of DOM within the Bay.

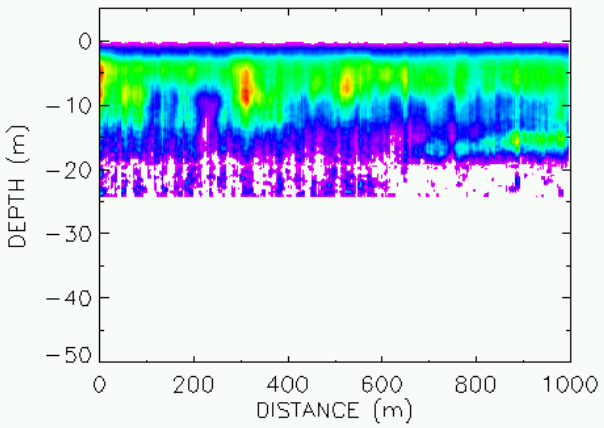

Figure 17. Echogram of nighttime layer in Zaikov Bay.

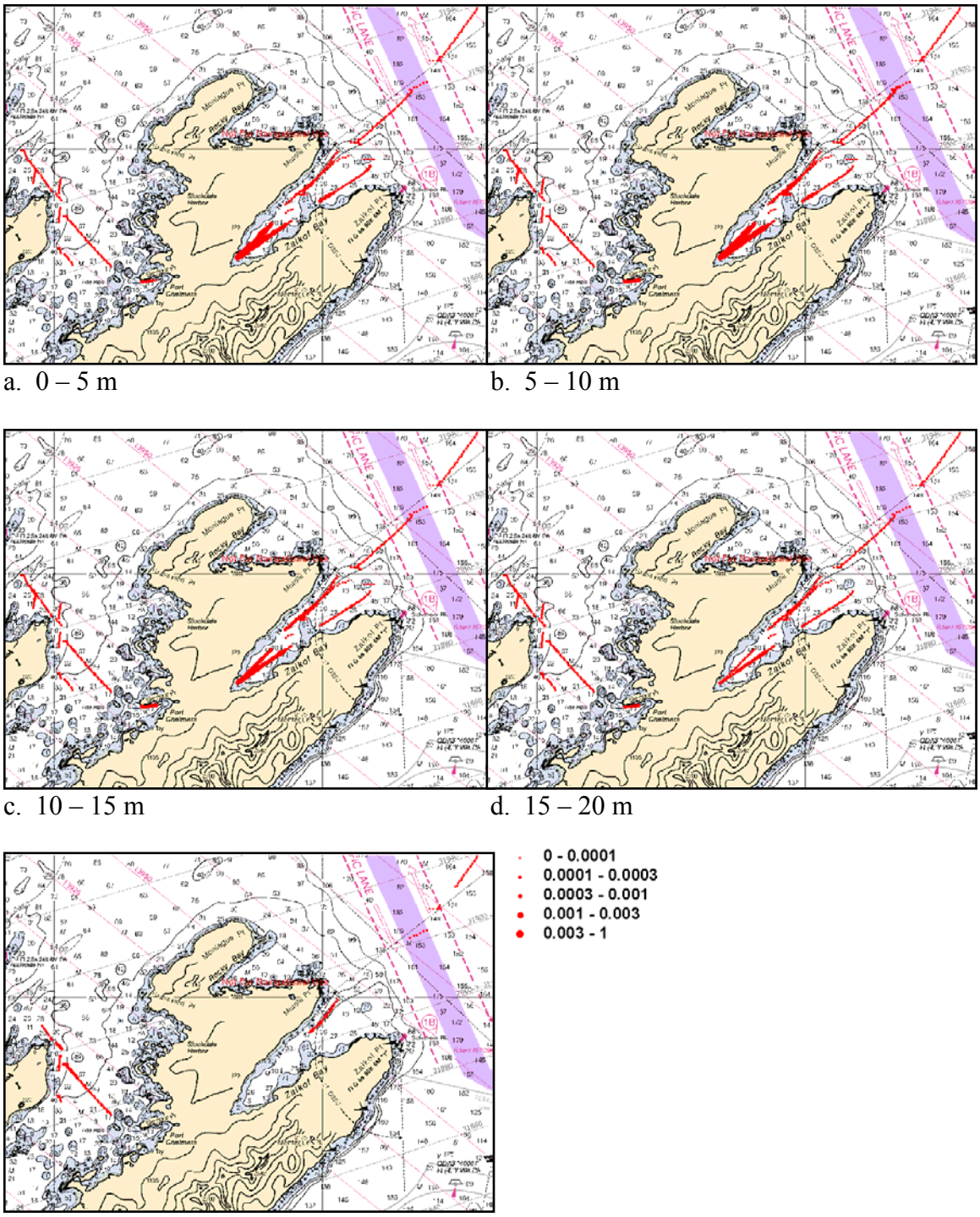

a. 0 – 5 m

b. 5 – 10 m

c. 10 – 15 m

d. 15 – 20 m

e. 20 – 25 m

Figure 13. Distribution of lidar energy by depth in and around Zaikov Bay for the day of March 22.

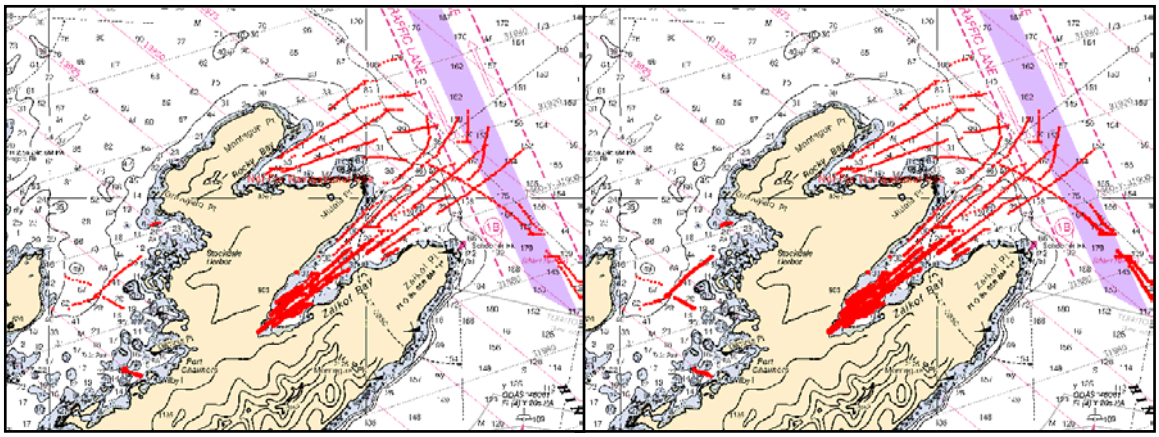

a. 0 – 5 m b. 5 – 10 m

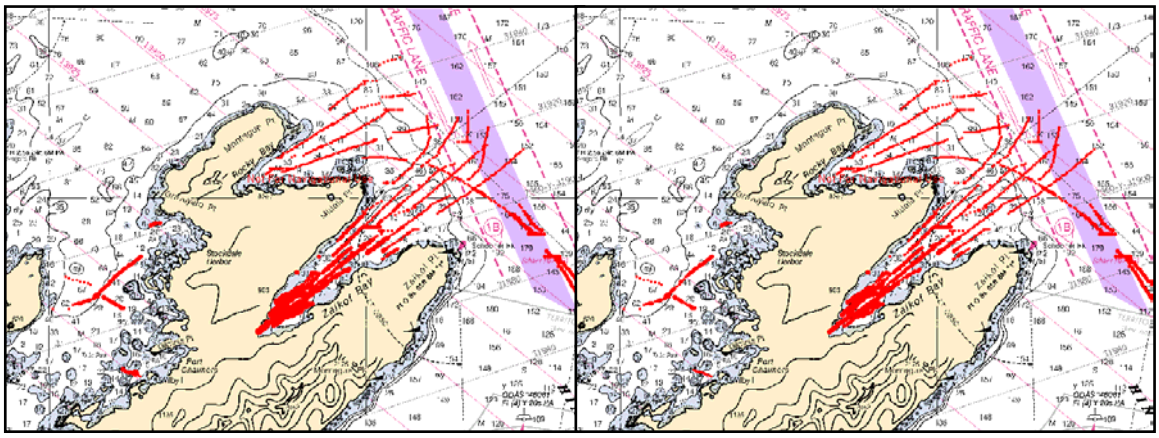

c. 10 – 15 m d. 15 – 20 m

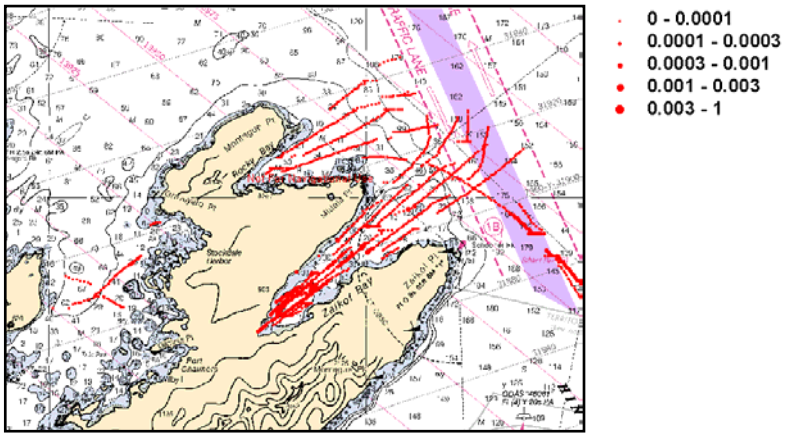

e. 20 – 25 m

Figure 14. Distribution of lidar energy by depth in and around Zaikov Bay for the night of March 21.

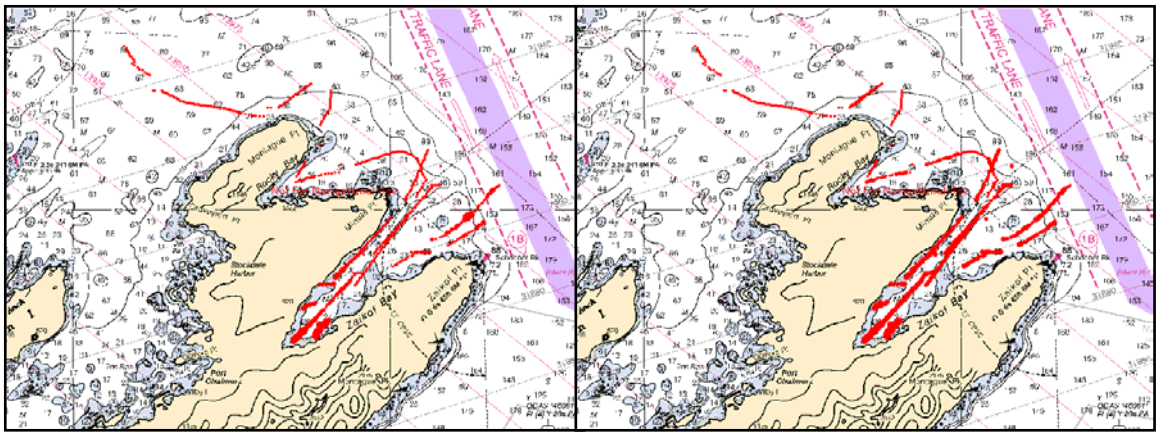

a. 0 – 5 m b. 5 – 10 m

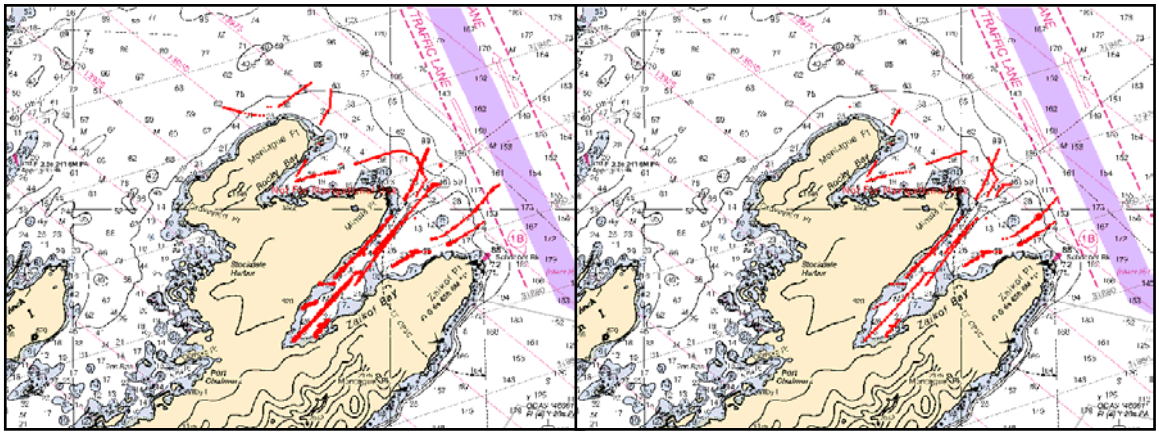

c. 10 – 15 m d. 15 – 20 m

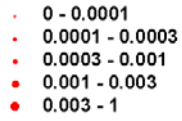

Figure 15. Distribution of lidar energy by depth in and around Zaikov Bay for the day of March 28.

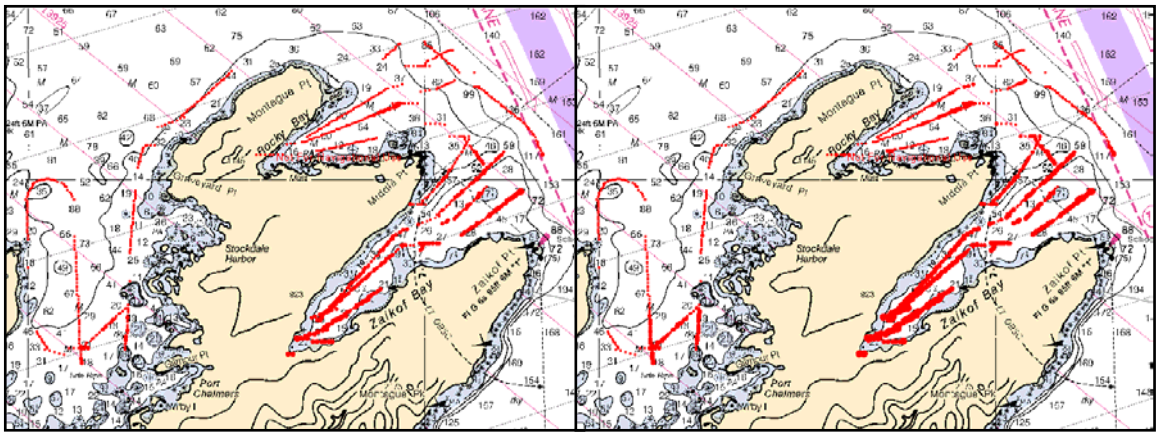

a. 0 – 5 m b. 5 – 10 m

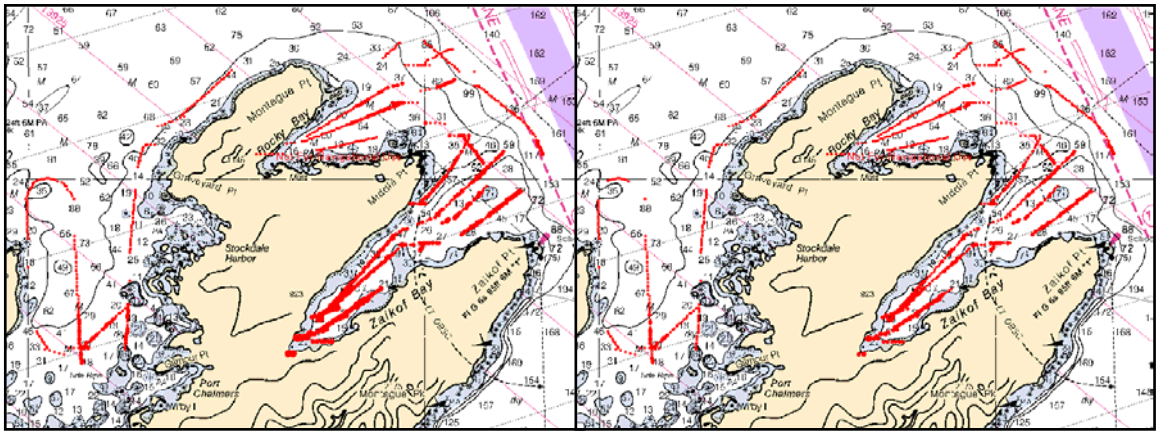

c. 10- 15 m d. 15 – 20 m

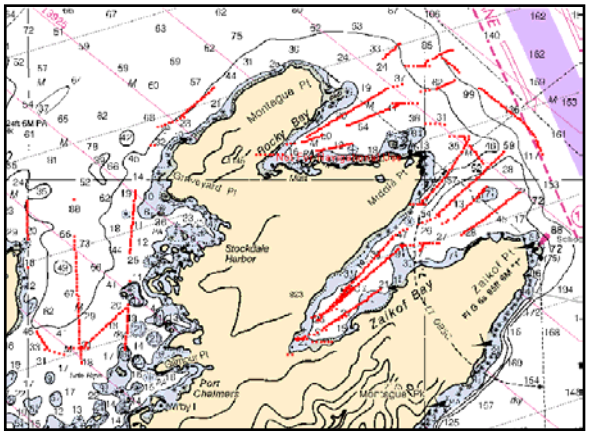

e. 20 – 25 m

Figure 16. Distribution of lidar energy by depth in and around Zaikov Bay for the night of March 29.

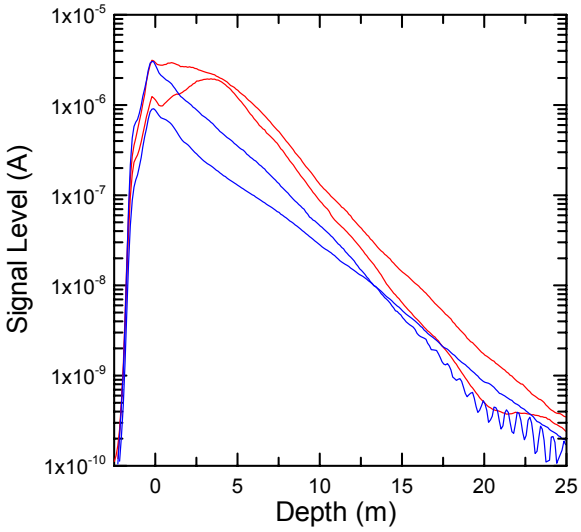

Figure 18. Average daytime lidar return along 1000 m within Zaikov Bay (red) and outside the bay (blue) for March 22 and 28. (Oscillation in lower blue curve is interference from marine radio.)

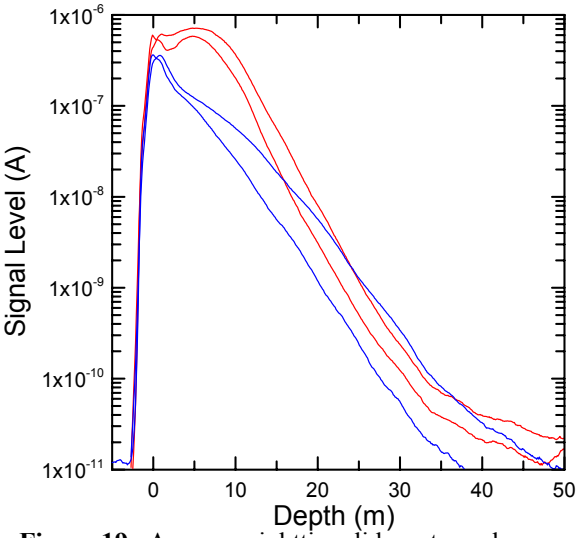

Figure 19. Average nighttime lidar return along 1000 m within Zaikov Bay (red) and outside the bay (blue) for March 21 and 29.

The point of this description of the lidar results from Prince William Sound is to demonstrate that the high absorption in the South Arm of Uganik Bay was not found everywhere. An over-wintering aggregation of herring in Prince William Sound that was very similar to the one in Uganik Bay was clearly detected by the lidar.

Thermal Images

The higher resolution thermal imager shows a great deal of detail. **Figure 20** is the thermal image of a group of birds on the surface. Individual birds are clearly resolved, although it is not possible to resolve any detail about them. The birds are warmer than the surrounding water surface, and show up as a lighter color. These birds are sitting on the surface. It is possible to tell whether they are sitting or flying by looking at subsequent frames. The position of flying birds changes relative to the background when they are flying. This is very easy to discern from the actual video display. While species identification is not possible, it is possible to identify alcids by their penchant for sitting in a line on the water. **Figure 21** presents an example. Images of birds are very common in the data.

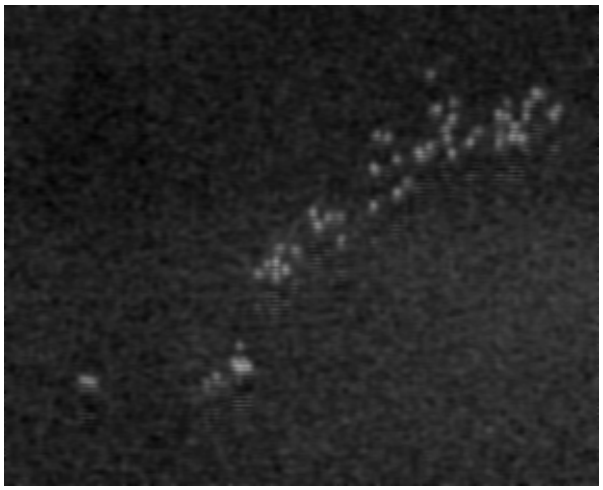

Figure 20. Thermal image of sitting birds

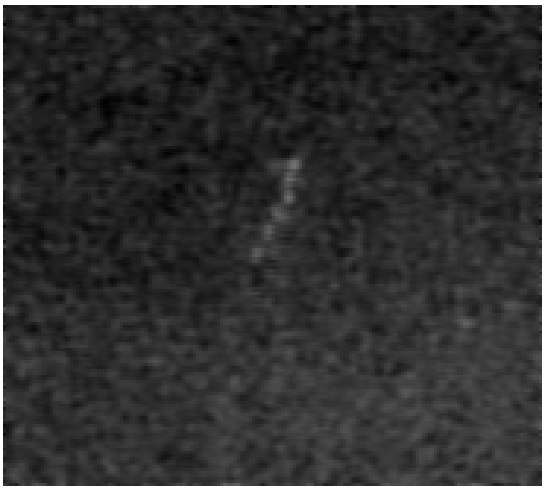

Figure 21. Thermal image of alcids

Images of sea lions are less common, and more difficult to identify. However, by comparing the thermal data with visual observations, we see a feature that seems to be indicative of sea lions moving through the water. An example is shown in **Figure 22**. This figure shows three warm spots that look similar to birds. However, each spot seems to be training a warm wake. We speculate that the bright spots are sea lion heads moving through the water. The wake is a disturbance of the cool skin that forms at the sea surface when the air temperature is cooler that the bulk water temperature.

Figure 22. Thermal image of sea lions with wakes

Looking at this type of signature in the infrared and the normal color signatures allow us to map the distribution of identifiable features in the images. **Figure 23** is a map showing the distribution of birds, alcids, swimming animals, and unidentified objects, or UFOs in the visible (green) and the infrared (red). In this figure, it is clear that most of the objects in the visible camera were not identifiable. Groups of birds were seen in the visible at several points in the Bay. In the infrared, all features that were seen were identified, although fewer features were seen. These included small groups of animals in Uganik Passage (a group of 4) and in South Arm (a group of 6). A group of 3 alcids and another group of 30 were observed off of West Point. Groups of sea lions and sea birds were seen visually that were not identified in the visible imagery. The reason is probably the flight altitude. The video system was designed assuming use of the Coast Guard

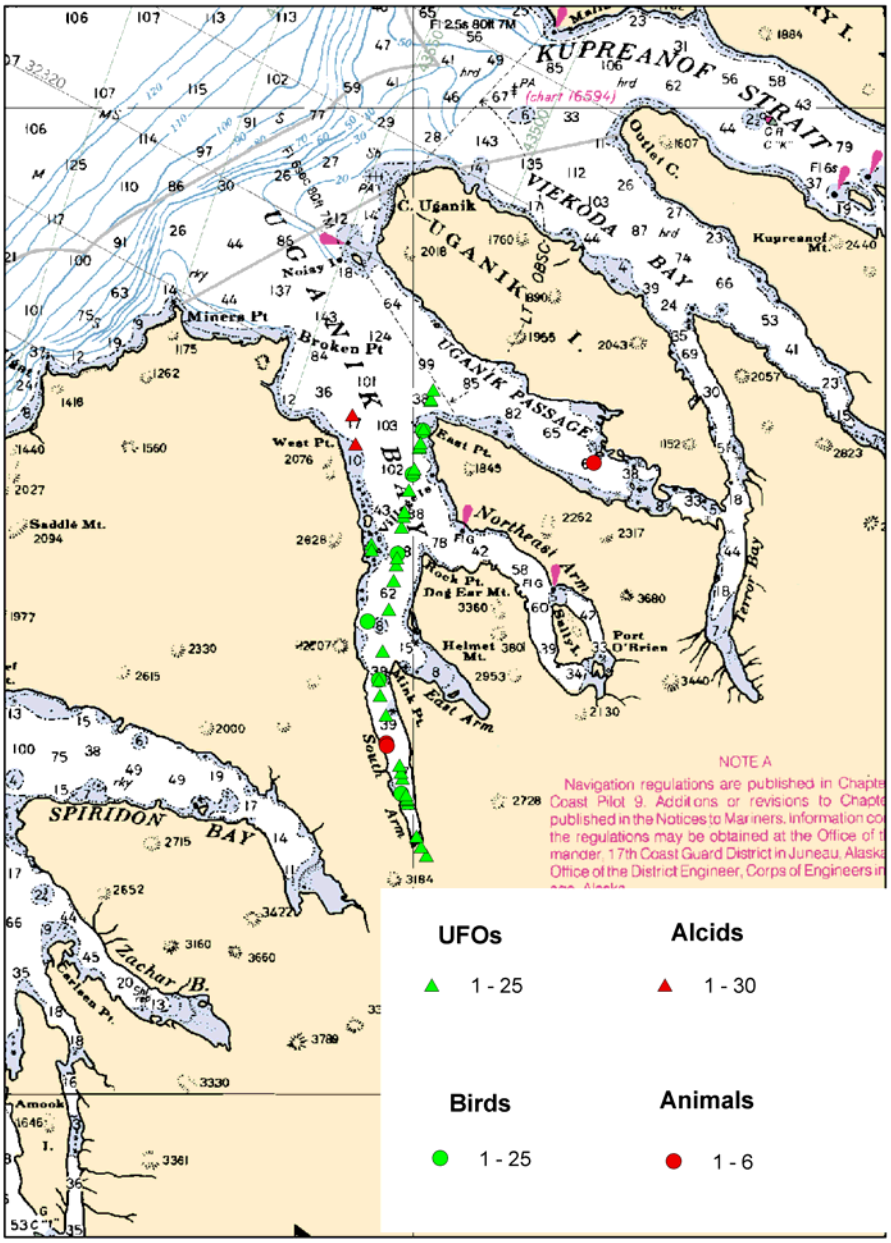

Figure 23. Map showing locations of groups of birds, animals, alcids, and unidentified objects (UFOs) in the visible (green) and infrared (red) images.

helicopter. The airplane had to fly much higher for safety reasons, so the effective resolution was much poorer.

Conclusions

While herring were detected by the lidar in Uganik Bay and Ugak Bay, the primary conclusion of this study has to be that the largest concentration of wintering herring, in the South Arm of Uganik Bay, could not be detected. This result was completely unexpected. A similar concentration of herring in a similar bay in Prince William Sound was detectable by the lidar. During the summer prior to this study, the lidar was used to map fish distributions in a variety of locations around Kodiak Island, including inside several bays. The South Arm of Uganik Bay was found to have a very high level of dissolved organic material, even when compared with the rest of Uganik Bay. This produced absorption of the laser beam that was greater than we have seen in any other area.

References

ANSI, 1993, *Safe Use of Lasers, Standard Z-136.1* (American National Standards Institute, New York).

Blough, N. V., O. C. Zafiriou, and J. Bonilla, 1993, "Optical absorption spectra of waters from the Orinoco River outflow: Terrestrial input of colored organic matter to the Caribbean," J. Geophys. Res. 98, 2271-2278.

Bricaud, A., A. Morel, and L. Prieur, 1981, "Absorption by dissolved organic matter in the sea (yellow substance) in the UV and visible domains," Limnol. Oceanogr. 28, 43-53.

Carder, K. L., R. G. Steward, G. R. Harvey, and P. B. Ortner, 1989, "Marine humic and fulvic acids: Their effects on remote sensing of ocean chlorophyll," Limnol. Oceanogr. 34, 68-81.

Churnside, J. H., Wilson, J. J, and Tatarskii, V. V., 2001, "Airborne lidar for fisheries applications," Opt. Eng., 40, 406–414.

Mobley, C. D., 1994, *Light and Water – Radiative Transfer in Natural Waters* (Academic Press, San Diego). p92.

Rosen, D.A.S. and A.W. Trites, 2000, "Pollock and the decline of the Steller sea lions: testing the junk-food hypothesis," Can. J. Zool. 78:1243-1250.

Thomas, G.L. and R.E. Thorne, 2001, "Infrared observations of nighttime predation by Steller sea lions," Nature 411, 1013; doi:10.1038/35082745.

H. M. Zorn, J. H. Churnside, and C. W. Oliver, 2000, "Laser safety thresholds for cetaceans and pinnipeds," Marine Mammal Sci. 16, 186-200.

Twardowski, M. S. and P. L. Donaghay, 2002, "Photobleaching of aquatic dissolved materials: Absorption removal, spectral alteration, and their interrelationship," J. Geophys. Res. 107; doi:10.1029/1999JC000281.